Fusion Engineering and Design 230 (2026) 115914

Contents lists available at ScienceDirect

Fusion Engineering and Design

journal homepage: www.elsevier.com/locate/fusengdes

IFMIF-DONES concrete neutron shielding benchmarks

Haridev Chohan [a,*], Martin Ansorge [b], Yuefeng Qiu [c], Tomasz Piotrowski [d], María José Martínez-Echevarría Romero [e], Ocean Wong [a,f], Ivan Kodeli [a], Joseph Neilson [a], Kimberley Lennon [a,f], Robin Smith [f,g], Radomír Běhal [b], Anastasia Cassisa [b], Vadim Glagolev [b], Daniil Koliadko [b], Ján Kozic [b,h], Jaromír Mrázek [b], Jan Novák [b], Eva Šimečková [b], Milan Štefánik [b,h], Callum Grove [a], Timothy Germany [a], Tim Eade [a], Mark Gilbert [a], Chantal Shand [a], Allan Harte [a]

[a] United Kingdom Atomic Energy Authority, Culham Campus, Abingdon, OX14 3DB, Oxon, UK
[b] Nuclear Physics Institute of the Czech Academy of Sciences, Řež, 250 68, Czechia
[c] Karlsruhe Institute of Technology (KIT), Karlsruhe, Germany
[d] Warsaw University of Technology, Al. Armii Ludowej 16, Warsaw, 00-637, Poland
[e] University of Granada, Campus Universitario de Fuentenueva (Edificio Politécnico), Granada, 18071, Spain
[f] School of Engineering and Built Environment, Sheffield Hallam University, Howard St, Sheffield, S1 1WB, UK
[g] Laboratory for Nuclear Science at Avery Point, University of Connecticut, Groton, CT 06340, USA
[h] Czech Technical University in Prague, Faculty of Nuclear Sciences and Physical Engineering, Department of Nuclear Reactors, V Holešovičkách 2, 180 00 Prague 8, Czechia

ARTICLE INFO

Keywords:
Neutron shielding
Neutronics
Benchmarking
Radiometrics
Concrete
IFMIF-DONES

ABSTRACT

Experiments have been performed to qualify the radiation shielding performance of concrete for the test cell of the IFMIF-DONES (International Fusion Materials Irradiation Facility - Demo Oriented NEutron Source) facility. A mock-up of ordinary concrete (OC) with local lime-dolomite aggregate was prepared, representing the structural concrete. Also, a mock-up of heavy concrete (HC) with magnetite aggregate was prepared, representing the radiation shielding concrete, particularly for removable biological shielding blocks inside the test cell. These mock-ups were irradiated by neutrons with a continuous energy spectrum up to 33 MeV using a fast neutron generator at the U-120M cyclotron facility at the Nuclear Physics Institute of the Czech Academy of Sciences, Řež. Activation foils were used for neutron diagnostics and were positioned throughout the mock-ups. There were five foil materials used: Au, In, Fe, Ti and Al. Gamma spectrometry of the foils was performed at the experimental site to measure the activities of the post-irradiation radionuclides. The experimental results are compared to calculated results obtained via radiation transport code modelling of the experiments and subsequent inventory code simulations of transmutation and activation. The comparison of calculated/experimental (C/E) results determines the confidence in the calculation methods to accurately represent the shielding performance of the concrete materials. Within the uncertainties, 100% of the OC results and 73% of the HC showed C/E agreement. Future calculations using these concretes should include safety factors of 2 and 3 for OC and HC respectively. The discrepancies for HC in particular should be considered in future calculations.

1. Introduction

IFMIF-DONES is a planned, accelerator-based, neutron irradiation facility, designed for the study and qualification of materials as part of the European roadmap to commercial energy from nuclear fusion [1]. Its purpose is to test materials under severe irradiation in a neutron field similar to that experienced in a fusion reactor first wall. It is an important facility in the preparation for post-ITER power plants, such as DEMO, since strong understanding of materials is vital for the design, licensing and reliable operation of such plants [1,2].

The test cell is the area within IFMIF-DONES in which material samples will be placed to be irradiated. Therefore, the test cell will experience high levels of neutron irradiation and so the structural and shielding materials used in the cell must be qualified. As part of the EUROfusion Early Neutron Source work package [3], two samples of concrete have been irradiated with neutrons to benchmark

* Corresponding author.
E-mail address: hari.chohan@ukaea.uk (H. Chohan).

https://doi.org/10.1016/j.fusengdes.2026.115914
Received 31 March 2026; Received in revised form 31 May 2026; Accepted 24 June 2026
Available online 1 July 2026

Glossary

IFMIF-DONES	International Fusion Materials Irradiation Facility - Demo Orientated NEutron Source
DEMO	DEMOnstration power plant
NPI-CAS	Nuclear Physics Institute of the Czech Academy of Sciences
E	Energy
n	neutrons
OC	Ordinary Concrete
HC	Heavy Concrete
FNG	Frascati Neutron Generator
SS	Stainless Steel
SINBAD	Shielding Integral Benchmark Archive and Database
PE	PolyEthylene
UKAEA	United Kingdom Atomic Energy Authority
CAD	Computer-Aided Design
NPS	Number of Source Particles
C/E	Calculated/Experimental
SDDR	ShutDown Dose Rate
TC	Test Cell
HPGe	High Purity Germanium
WW	Weight Window
SSR/W	Surface Source Read/ Write

their shielding response to inform the design of the IFMIF-DONES test cell.

A sample of ordinary concrete prepared with local lime-dolomite aggregate was benchmarked for the structural concrete. Also, a sample of heavy concrete prepared with magnetite aggregate was benchmarked for the radiation shielding concrete, particularly for removable biological shielding blocks inside the test cell. Mock-ups of both of these concretes were prepared and irradiated with neutrons with the U-120M cyclotron at NPI-CAS, Řež. Activation foils were used to measure the neutron attenuation through the mock-ups. Computational models of the experiments were developed and simulations were performed to replicate the experiments. C/E results were obtained including uncertainties which were quantified through dedicated sensitivity and uncertainty analyses.

2. Methodology

2.1. Irradiation facility

The neutron spectrum of IFMIF-DONES will have a broad peak around 14 MeV and extend up to 55 MeV. It will produce maximum fluxes of 10^{15} n/cm^2/s [2]. As part of the European roadmap commercial energy from fusion, IFMIF-DONES was recommended to be built as there was a requirement for a facility that could generate both high-energy neutrons and high neutron fluxes [1]. As such, existing facilities are inferior to IFMIF-DONES in these aspects. Nevertheless, materials still need to be benchmarked for the design and construction of IFMIF-DONES itself. The U-120M cyclotron at NPI-CAS, Řež, is capable of generating a continuous spectrum of neutrons up to 33 MeV and neutron fluxes of up to 10^{11} n/cm^2/s. The cyclotron accelerates protons up to 35 MeV which impinge, in this scenario, onto an 8 mm thick beryllium target to produce neutrons. The neutron spectrum has been previously characterised [4]. Both spectra are shown in Fig. 1.

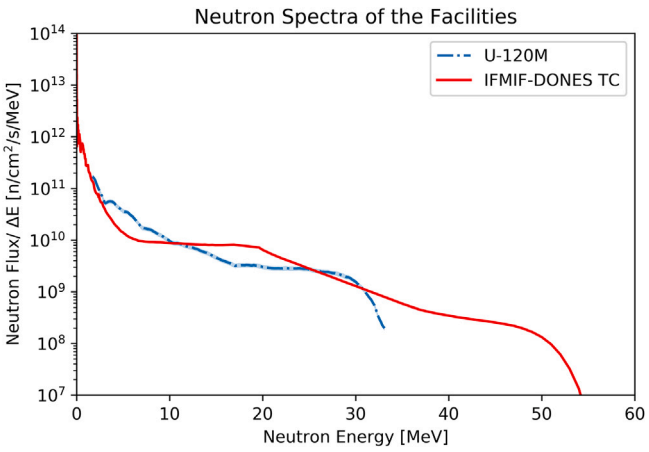

Fig. 1. The neutron spectra of U-120M [4] and the IFMIF-DONES Test Cell.

Table 1
Concrete compositions used in the experiments.

Element	OC abundance [Weight %]	HC abundance [Weight %]
H	0.35	0.30
C	10.29	–
O	49.66	28.60
Na	–	0.18
Mg	9.87	0.27
Al	0.75	0.69
Si	1.99	2.57
P	–	0.45
S	1.07	0.13
Cl	0.02	0.01
K	0.06	0.17
Ca	24.16	4.7
Ti	0.05	0.03
Fe	1.73	61.9
Theoretical Density [g/cm^3]	2.55	3.94

2.2. Concrete test samples

Concrete test samples were prepared for the IFMIF-DONES test cell specification, following the ITER concrete Refs. [5]. The OC samples were prepared with a lime-dolomite aggregate from local sources for the structural concrete samples. A magnetite aggregate was used for the radiation shielding HC samples. After investigations of raw materials, a group of prebatches were prepared and technical properties — density of compressive strength, were measured. The samples for the Řež irradiation experiments were prepared according to the dimensions established by the mock-up design pre-analysis (see Section 2.3). The final compositions of the samples used are described in Table 1.

2.3. Mock-Up design

Previous neutron shielding benchmark experiments, such as the 2016 FNG copper benchmark [6] and the 1995 FNG SS shielding benchmark [7], were used to guide the concrete experiments and to benefit from the previous experience. These benchmarks and others are documented in the SINBAD database [8].

Nuclear analysis parametric studies were performed to determine the dimensions of the mock-ups. Using MCNP [9], radiation transport models of cuboidal mock-ups positioned in the U-120M experiment hall

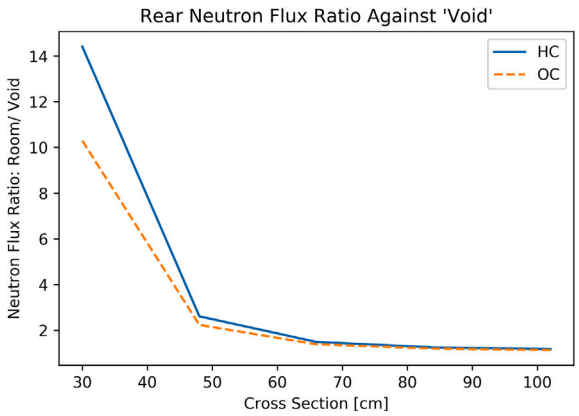

Fig. 2. The total neutron flux at the back of the mock-ups divided by the equivalent flux without the experimental hall modelled, as a function of cross-section.

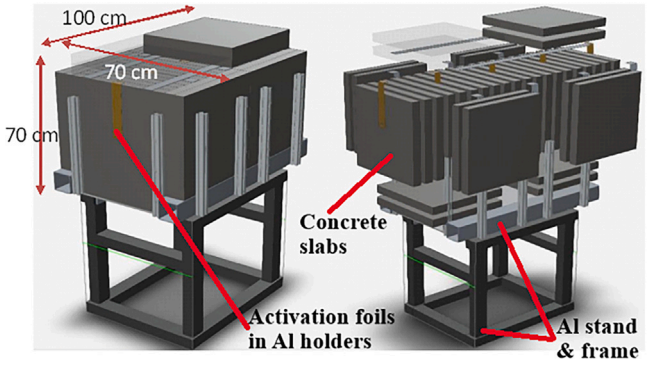

Fig. 3. The final design of the concrete mock-ups including support structure and diagnostic holders. Normal view (left) and exploded view (right).

were created to simulate the neutron transport in and around the mock-ups. Full details regarding the simulations can be found in Section 2.7. The cross-sectional area perpendicular to the beam-axis, and the mock-up depth were independently varied, and the neutron flux results were compared.

The depth of the mock-ups was required to be great enough to provide significant neutron flux attenuation, at least a couple of decades of attenuation, so that the neutron shielding properties of the concretes were able to be thoroughly investigated. The mock-ups' depths also need not be greater than the depth at which the neutron flux becomes so low that it is difficult to measure.

The determination of the mock-up cross-section depended on a number of factors. The neutron beam had some angular and spatial spread, the mock-up cross-section had to be large enough to capture that spread. Furthermore, it was desirable to observe as much bulk physics phenomena as possible, in other words, it was desirable that the neutrons underwent many interactions within the sample which is aided by an increased cross-section. Neutrons can scatter from the experimental hall and into the mock-up which interferes with the neutron flux results, ideally the mock-up would be isolated from the room. Increasing the cross-section helps to reduce the contribution of room-scattered neutron to the results because, as explained, more of the neutron beam is incident into the mock-up and less neutrons escape the mock-up sides since there are more interactions within the mock-up. In addition, an increased cross-section provides more shielding against room-scattered neutrons.

The effect the mock-up cross-section on the room-scatter is shown by the results of one of the parametric studies, in Fig. 2. In this study, for a fixed mock-up thickness of 100 cm, the mock-up cross-sections were varied from 30 cm × 30 cm to 100 cm × 100 cm. For each cross-section, the mock-ups were modelled in the full experimental hall ('room') and also in a 'void' to represent the ideal scenario with no room-scatter. The neutron fluxes in a small volume at the back of these mock-ups were tallied and the ratios of the 'room':'void' models are plotted. The plot shows a steep drop-off which softens after around 50 cm × 50 cm and tends towards unity which would represent zero room-scatter contribution. There was little improvement after around 66 cm × 66 cm.

Another way to mitigate room-scatter interference is to use external shielding to isolate the mock-up from the experimental hall. Polyethylene and cadmium were investigated for shielding the mock-ups. Both are common neutron shielding materials and have been used in benchmarks previously [8,10,11], and they were readily available to be used in these experiments. Polyethylene has a high hydrogen content and so is an effective neutron moderator while cadmium has a high thermal-neutron absorption cross-section. Simulations were performed with these shielding materials.

A disadvantage of using extrinsic shielding in such an experiment is that even though the shielding reduces the contribution of the room-scattered flux to the results, it risks adding its own contribution of flux that has scattered off and inside the extrinsic shielding itself. Since the extrinsic shielding would be positioned directly outside of the mock-up, the likelihood of contributing a 'shield-scatter' component to the flux results is high. The mock-up, therefore, does not become truly isolated from the surroundings, but the experiment becomes a benchmark of the mock-up plus shielding set-up. This was also investigated by the simulations.

Ultimately, based on the simulations, dimensions of 70 cm × 70 cm × 100 cm were determined to be necessary for the mock-ups. Extrinsic shielding was decided against because the simulations predicted that the neutron shielding provided was not enough to outweigh the additional uncertainties introduced by the shielding material.

To ensure uniformity and structural integrity of the concrete samples, the maximum dimensions that were able to be manufactured to optimise the cross-sectional area were 50 cm × 50 cm × 5 cm. Therefore, a layered design for the mock-ups was adopted, consisting of 20 concrete samples to give an overall depth of 100 cm. A cross-section of 50 cm × 50 cm was less than recommended from the pre-analysis. Consequently, two layers of concrete samples were added transversally around the sides of the mock-ups which effectively increased the cross-sectional area to 70 cm × 70 cm which was in line with the conclusions from the pre analysis. These transversal samples also provided the benefit of covering the streaming paths between the layers of the main part of the mock-ups. The final mock-up design is shown in Fig. 3.

2.4. Diagnostics

Activation foils were chosen as the sole diagnostic for the experiments. Activation foils work by becoming activated under neutron irradiation. The activation products then decay after the irradiation and emit gamma radiation. Gamma spectroscopy is then used to determine the energy and number of gamma rays. This information is used to work backwards to determine the activity of the foil products and thus the neutron fluence and spectrum.

Foils are non-invasive so they could be positioned freely throughout the mock-ups without taking up much space nor disrupting the mock-up structure. Activation foils are passive and require no electronics that could be disrupted in the harsh neutron fields and so they are rad-hard and easy to use. Activation foils have often been the primary diagnostic in similar benchmark experiments for these reasons [6,8].

There was a limited range of foils that were available for these experiments and these were assessed on a variety of factors to determine

Table 2
The dominant neutron-activation reactions for the selected foils and their details.

Reaction	Product half-life	Reaction threshold [MeV]
^{56}Fe (n, p)^{56}Mn	2.58 h	3.0
^{27}Al (n, α)^{24}Na	15.0 h	3.2
^{48}Ti (n, p)^{48}Sc	43.7 h	3.3
^{48}Ti (n, np)^{47}Sc	3.35 days	12
^{197}Au (n, γ)^{198}Au	2.70 days	–
^{115}In (n, n') ^{115m}In	4.49 h	0.34

which could be applied successfully. The threshold energies for the activation reactions determined whether the reactions would occur under the neutron irradiation, also it was required to use a range of foils with a range of threshold energies to be able to investigate the full range of the neutron spectrum. Analysis was performed to determine whether the foils would become activated enough to give statistically significant (<1% statistical uncertainty) counts in the gamma spectroscopy using the Currie minimum detectable activity equation [12]. This analysis required the neutron fluence and spectra received by the foils during the irradiation, which was determined using MCNP [9] for radiation transport simulations. The neutron spectra was input into the FISPACT-II [13] activation calculations to determine the activities of the foil products. The activities were used along with the half-lives, gamma-ray branching ratios, gamma-ray energies and gamma spectrometer detection efficiencies to calculate the counts that would be observed. Full details regarding the simulations can be found in Section 2.7. This analysis was aided with the Foil Selector tool [14] and also UKAEA and NPI-CAS activation foil experience, particularly NPI-CAS experience with foils for the U-120M cyclotron. The final selection of foils and their primary neutron-activation reactions are listed in Table 2.

Although the foils were selected to span the range of neutron energies, the selection was not optimised for spectrum unfolding as this was not the intention of the experiments. The secondary reactions of the foils would need to be investigated to see if there are sufficient pathways for reliable unfolding.

Two HPGe gamma spectrometers were available for the OC experiment and three for the HC experiment.

2.5. Experimental planning

In order to optimise the experiments and extract as much information out from them as possible, pre-analyses were performed to determine the irradiation times of the experiments and the scheduling for the gamma spectroscopy.

Radiation transport calculations and activation and inventory calculations were used to inform the planning (see Section 2.7). In these calculations, 'sufficient' activation of the activation foils was determined as the activation required to give 1E+4 gamma spectroscopy counts for the primary gamma peak. This number of counts corresponds to 1% counting statistical uncertainty. Funding enabled just over a day of irradiation for each experiment. The foils with non-threshold reactions or that were easily activated did not require much beamtime to become sufficiently active. Therefore, the calculations predicted that Au and In foils at all depths would become sufficiently activated after a short irradiation of 2 h. The limited neutron attenuation from depths 0–40 cm meant that the neutron flux was high enough at these depths to sufficiently activate all of the foils also with a short irradiation of 2 h. 2 h was enough time for the cyclotron to ramp-up to its peak current and run steadily. For the remaining foils (Al, Fe and Ti) at depths greater than 40 cm, the calculations determined that 24 h of irradiation was required to give sufficient activation. Therefore, it was planned to split the irradiations up into two parts: an initial 2-hour irradiation after which the sufficiently activated foils were extracted; and a subsequent 24-hour irradiation for the remaining foils.

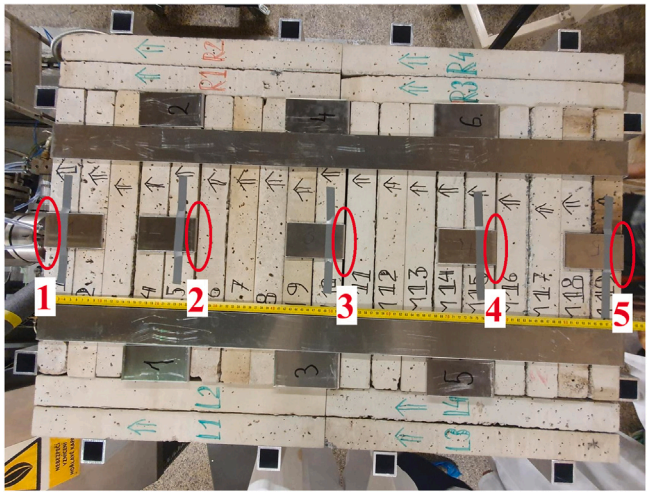

Fig. 4. The OC mock-up from above with the top concrete samples removed. The diagnostic positions are labelled.

In addition to optimisation of the experiment from a scientific perspective, radiation safety was also considered in the experimental planning. SDDR analysis was performed using MCR2S [15] to calculate the dose environment in the cyclotron hall after the irradiations. This confirmed that the dose rates were below the limits in the hall after both the 2- and 24-hour irradiations so that workers could enter and extract the foils.

In ideal conditions, there would be a gamma spectrometer for each foil so the foils could be measured immediately after extraction, limiting the decay times. This, however, is unrealistic and in these experiments 2 and 3 gamma spectrometers were available for the OC and HC experiments respectively. Therefore, the gamma spectroscopy of the foils had to be scheduled. Splitting the irradiations up into 2 alleviated some of the demand on the gamma spectroscopy. The scheduling was determined based on the activities and the half-lives of the foils. The foils containing shorter-lived activation products were prioritised. Foils with higher activities were also prioritised so that they could be quickly measured and then more time could be spent measuring the foils with lower activities. Gamma spectroscopy schedules were made based upon simulations to enable sufficient counts to be measured for every foil.

2.6. Experiments

The ordinary concrete experiment was performed in Řež in March 2023 and the heavy concrete experiment was performed in June 2023. Due to the manufacturing process, the concrete samples had rough surfaces which increased their effective thicknesses compared to the design. The mock-up support structure was designed to house a mock-up with total depth of ~ 100 cm. Therefore, to fit in the support structure, the ordinary concrete mock-up became 19 samples deep and the heavy concrete mock-up became 18 samples deep. The activation foils were positioned approximately in the planned positions, accounting for the real sample thicknesses. For the OC experiment, the foil depths were every 25 cm and all 5 types of activation foil were placed at each depth. For the HC experiment, more activation foils of the same materials became available and so foils were placed in three additional depths spread between 25 cm and 100 cm where there was more uncertainty in the OC results. The mock-ups and diagnostic locations are shown in Figs. 4 and 5.

The depths of the activation foil locations are listed in Table 3.

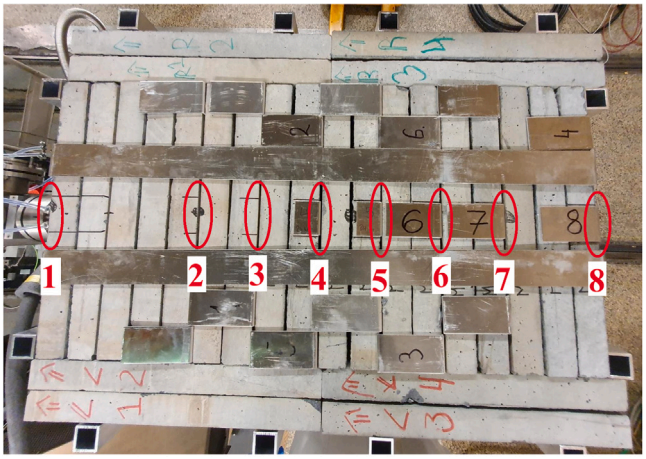

Fig. 5. The HC mock-up from above with the top concrete samples removed. The diagnostic positions are labelled.

Table 3
The depths of the activation foils in the experiments.

Location number	OC depth [cm]	HC depth [cm]
1	0	0
2	26	26
3	52	37
4	78	48
5	100	59
6	–	70
7	–	81
8	–	97

Following the irradiation planning, the mock-ups were irradiated for 2 h, followed by approximately 1 h to change the foils and then a 24-hour irradiation.

Post-irradiation gamma spectroscopy was performed using the planned schedule as a guide. The radiometric scientists used their judgement to optimise the measurements as they went. Two HPGe spectrometers were used for the OC measurements, one recorded in list-mode or time-correlated event data and the other recorded time-integrated spectrum data. For the HC experiment an extra list-mode HPGe spectrometer was used. The time-integrated spectrum data was analysed using the commercial software package, Genie [16], and the list-mode data was analysed using the NPI-CAS Gregory software package [17]. Gregory produces time-integrated spectrum data from the list-mode data. These software packages were used to make fits on the gamma peaks. Self-absorption was accounted for and the actual masses of the foils were used.

The dimensions of the foils are presented in Table 4, following the logic that the deeper the position, the lower the neutron flux and so larger foils were used. In all positions the foils were stacked in front of one another in the order shown in the table, i.e. Fe, Al, Ti, Au, In. The logic for this ordering was to have the most easily activated foils towards the back (Au and In), to reduce the effect of shielding from other foils.

The neutron yields of the irradiations were indirectly monitored by the proton current, the yields of the irradiations are listed in Table 5.

2.7. Simulations

All radiation transport simulations were performed using MCNP 6.2 [9]. The U-120M cyclotron hall MCNP model was provided by NPI-CAS. The mock-up designs were made in CAD and converted into

Table 4
The thicknesses of the foils in the experiments [mm]. The diameter of the foils was 15 mm except for those marked with '*' which had diameters of 25 mm.

Position	OC					HC				
	Fe	Al	Ti	Au	In	Fe	Al	Ti	Au	In
1	0.08	0.10	0.47	0.04	0.25	0.08	0.49	0.47	0.04	0.09
2	0.08	0.10	0.52	0.04	0.26	0.49	0.49	0.52	0.04	0.25
3	0.08	0.10	0.52	0.04	0.26	0.49	0.49	0.52	0.04	0.26
4	0.49	0.49	0.52	0.05	0.66	0.49	0.49	0.52	0.05	0.26
5	0.49	0.49	0.52	0.05	0.78	0.50	0.49	0.52	0.05	0.49
6	–	–	–	–	–	0.94*	0.96	1.03	0.05	0.50
7	–	–	–	–	–	0.94*	1.02*	1.03	0.05	0.66
8	–	–	–	–	–	0.96*	1.03*	1.03	0.05	0.78

Table 5
The neutron yields of the irradiations.

Irradiation	OC	HC
2-Hour	4.4E+17	4.7E+17
24-Hour	5.5E+18	5.5E+18

MCNP format using TopMC [18]. The activation foils were explicitly modelled in the MCNP geometry to account for self-shielding of the foils themselves. Plots of the MCNP models are shown in Figs. 6–9. Variance reduction was performed with a targeted mesh global WW using ADVANTG [19]. A global WW was used to get good statistics for scattered neutrons in the room to ensure that their contributions to the fluxes in the foils was accounted for. A local WW would have placed less importance on the room-scattered neutrons. The source was previously characterised [4]. The source was modelled by simulating protons born from the cyclotron and then transporting the neutrons created from the proton reactions in the beryllium target. To make the simulations less computationally intense, the simulations were split into two parts: the proton transport and the generation of neutrons in the beryllium target, and subsequently the transport of neutrons. This was enabled using the MCNP SSR/W capability. The proton run was run to 5E+10 NPS, this was limited by the size of the surface source file that was written. This corresponded to approximately 2E+9 neutron histories. The SSR/W capability conserves the neutron particle track weights from the proton source calculation and propagates them into the neutron source calculation to provide complete statistical uncertainties in the results from both calculations. The MCNP manual [9] states that more histories in the SSR simulation can be run than were recorded in the SSW simulation, with appropriate recalculation of the particle weights. Unfortunately, this capability was not observed and the SSR simulation was limited to the number of histories recorded in the SSW simulation. Therefore, using this source method meant that more neutron histories could not be simulated to improve statistical convergence. The unfolded experimental spectrum reported in the source characterisation [4] was investigated for use in these analyses, however, since it was obtained under different experimental conditions, its direct application as a source term here was not straightforward and was therefore not adopted. Replicating the surface source as a standard MCNP SDEF source was also investigated but initial results were not accurate enough for these purposes and so it was abandoned in the interest of time. The ENDF7PROT nuclear data library was used for proton transport [20] and the FENDL-3.2b library was used for neutron transport [21]. The neutron spectra in the activation foil cells were tallied with cell tallies using the CCFE-709 energy group structure [22]. Reaction rate tallies were also included on the foil cells to determine the reaction cross-sections using the IRDFF-II dosimetry library [23].

The neutron spectra and reaction cross-sections obtained from the radiation transport simulations for the foils were then used in FISPACT-II to calculate the activity of the foils at decay times corresponding

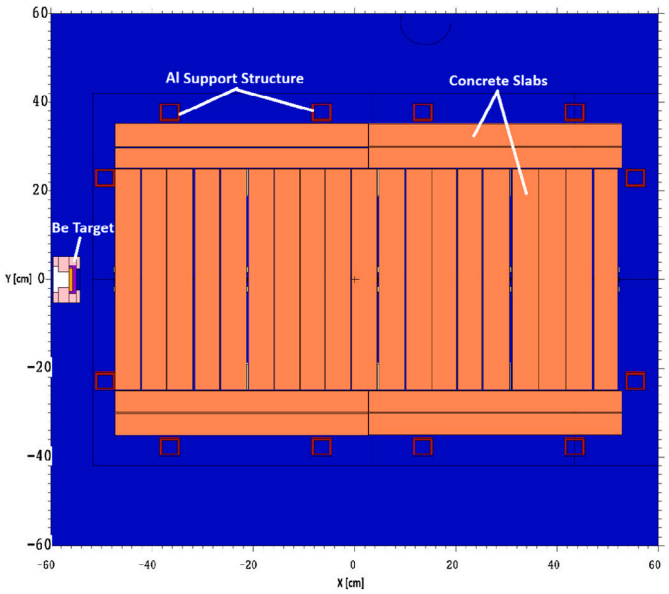

Fig. 6. A slice in the vertical Z-plane of the MCNP model of OC.

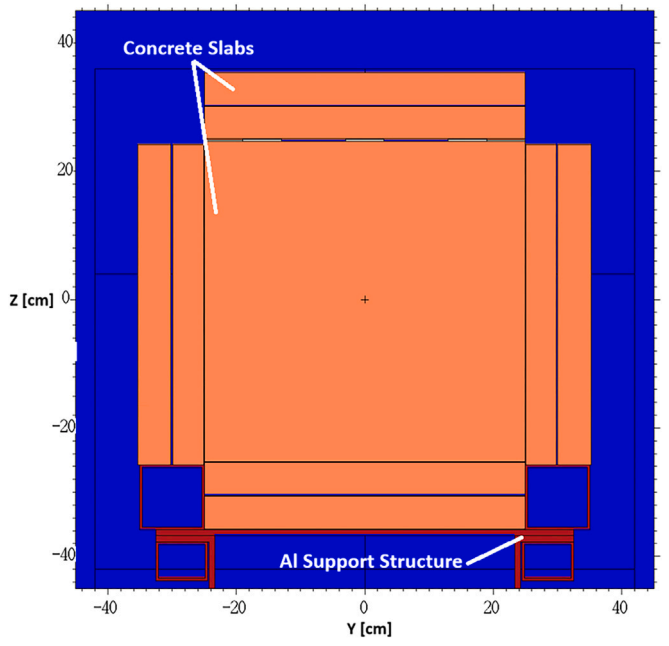

Fig. 7. A slice in the X-plane of the MCNP model of OC.

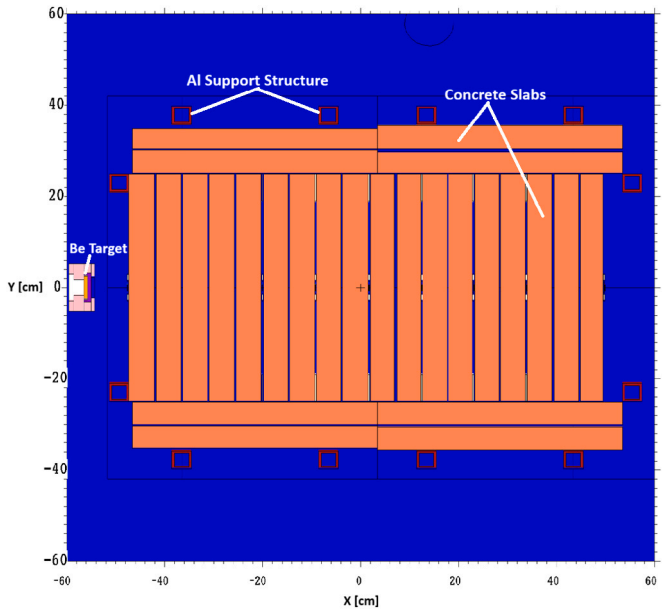

Fig. 8. A slice in the vertical Z-plane of the MCNP model of HC.

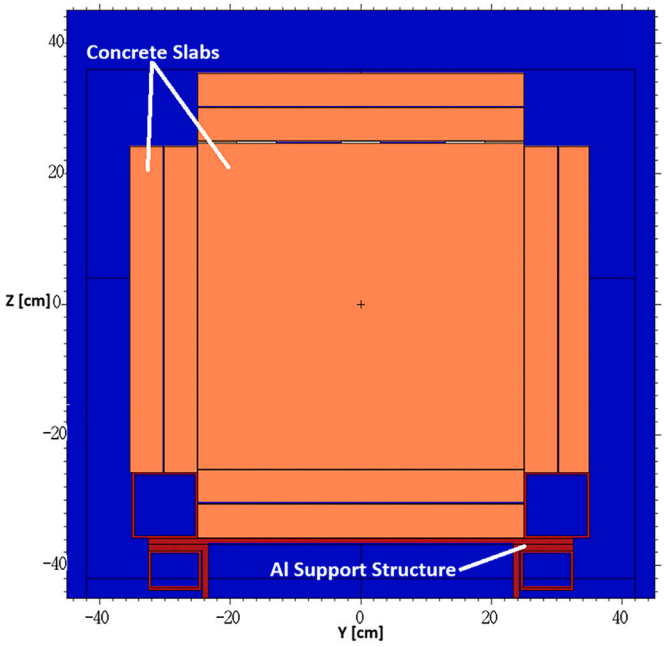

Fig. 9. A slice in the X-plane of the MCNP model of HC.

to the gamma spectroscopy measurement times. All secondary reactions not included in Table 2 were calculated using the TENDL-2017 library [24] in FISPACT-II.

2.8. Sensitivities and uncertainties analysis

Analyses were performed to quantify the uncertainties in the modelling of the experiments and the sensitivity of the results to these variables. The sources of uncertainty were:

1. Density of the concrete samples.
2. Geometrical modelling accuracy of the mock-ups. I.e. the modelled gap sizes between the slabs.
3. Distance to the neutron source.
4. Characterisation of the neutron source.
5. Neutron transport library.
6. Nuclear cross-section data.

Other sources of uncertainty were considered but were deemed negligible compared to the six sources of uncertainty listed. For example, the positions of the activation foils were measured accurately at the time of the experiments and photographic evidence was recorded for reference. The uncertainties on these measurements were ± 0.5 cm, which was negligible compared to the other sources of uncertainty.

For the continuous variables 1–3, bounding scenarios were established for each variable and the simulations were performed for these scenarios, changing each variable independently. The results from these

Table 6
The continuous sources of uncertainty and their bounds.

Source of uncertainty	OC		HC	
	Lower	Upper	Lower	Upper
Concrete density [g cm^{-3}]	2.36	2.55	3.90	3.97
Gaps between slabs [mm]	0	3.2	0	4.1
Source distance [cm]	5.8	7.5	5.8	7.5

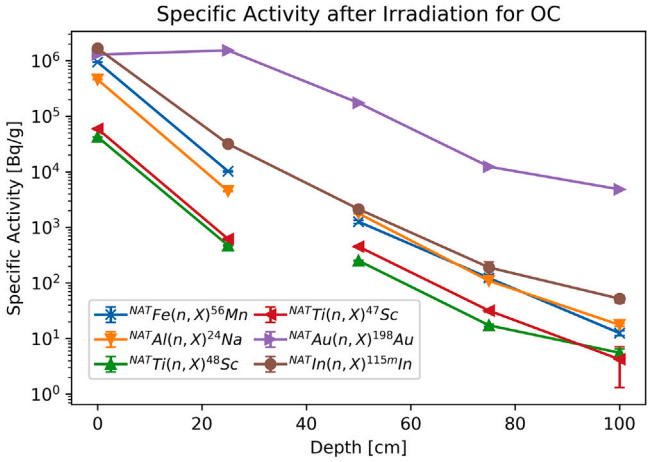

Fig. 10. The experimental specific activities of the foil activation products, immediately after irradiation for OC. The discontinuities are due to the different irradiations.

simulations determined the upper and lower bounds for the uncertainties due to each variable. The bounding scenarios are listed in Table 6. The bounding scenarios were determined by on-site measurements and, in the case of the concrete density, also factored in the supplier's data. The calculations were simple upper–lower bound simulations where flat distributions between the bounds were implicitly assumed.

For the discrete variables 4 and 5, different nuclear data libraries were investigated. For the proton transport, both the ENDF7PROT and JENDL-4.0/HE [25] libraries were used, as in the original characterisation [4]. For the neutron transport, both the FENDL-3.2b [21] and JEFF-3.3 [26] libraries were used. FENDL-3.2b is the reference neutron transport library for EUROfusion DONES neutronics and JEFF-3.3 was used as a comparison.

The sensitivity and uncertainty due to the nuclear cross-section data was investigated in more detail courtesy of independent analysis [27]. The analysis used SUSD3D/XSUN-2023 [28–30] to calculate the sensitivities to the basic nuclear data cross sections and other uncertainties such as water and impurity content.

3. Results

3.1. Experimental results

The experimental activities of the activation products of the foils were calculated using the gamma spectroscopy measurements. The activities immediately after the irradiations were back-calculated and are shown in Figs. 10 and 11 for OC and HC respectively. The uncertainties were calculated by the gamma spectroscopy software and include contributions from counting statistics, detector efficiencies, sample quantities and branching ratios [16].

The activities exhibit general exponential decay trends for the same irradiation times. The Au foils exhibit differences compared to the other foils, the attenuation is less than the other results and the activities in the second positions are higher than the exponential trends would

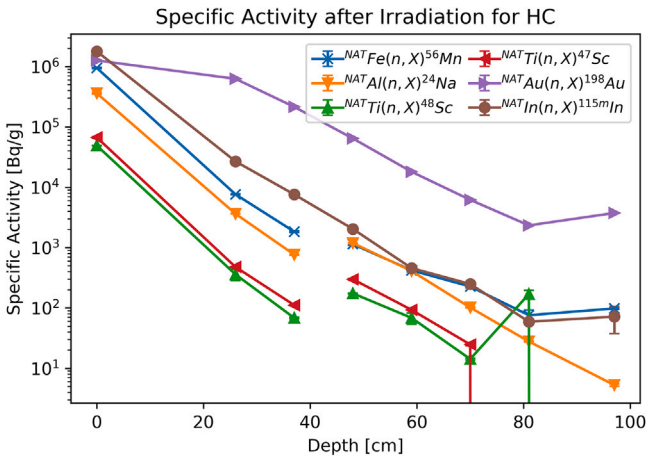

Fig. 11. The experimental specific activities of the foil activation products, immediately after irradiation for HC. The discontinuities are due to the different irradiations.

suggest. This is due to the dominant Au reaction being the only non-threshold reaction and, therefore, it is sensitive to thermal neutrons. The high energy neutrons are moderated to thermal energies by the concretes which gives the observed increase in the activity in the second position for OC compared to the first position and the increase in the activity in the second position for HC compared to that expected from the exponential trend. As well as moderated neutrons, scattered neutrons will also have low energies and contribute to the Au reaction, this is why the Au activity decreases less than those due to threshold reactions.

Another observed deviation from the exponential trends is the increase in activity of all foils towards the back of the mock-ups, this is more pronounced in HC and more obvious due to the increased granularity of the HC results. This activity increase is due to back-scattered neutrons re-entering the rear of the mock-ups. The higher rear activities in HC suggest poorer shielding for scattered neutrons, although the rest of the results show similar neutron attenuation for both concretes.

The activity at 81 cm for ^{48}Sc in HC shows an unusually large increase that cannot be accounted for by scattered neutrons because they would affect the non-threshold reaction more. The dominant reaction for this foil has a threshold of 3.3 MeV. The ^{27}Al (n, α) ^{24}Na and ^{56}Fe (n, p) ^{56}Mn reactions have a similar thresholds of 3.2 and 3.0 MeV respectively but relatively high activities for those foils were not observed at this position. The simulation results for the ^{48}Sc activity also did not predict such a relatively high value, see Fig. 17. The spectrometry analysis was independently reviewed and no errors were found. Background gamma spectrometer measurements were made at the time of the foil measurements to isolate the gamma lines due to the foils. However, it is possible that the cause of this large activity was still due to the spectrometry rather than the neutron transport, since this result was not corroborated by the other foils.

In each experiment, the irradiations were split up into two parts so that different foils were irradiated for different amounts of times, as explained in Section 2.5. Therefore, the activities of the foils from different irradiations cannot be directly compared to investigate the attenuation. This is represented by the discontinuities in the plots in Figs. 10 and 11. Therefore, in order to investigate the attenuation of the concretes, the asymptotic saturated activities were calculated to extrapolate the activities of all foils out to 24 h of irradiation, factoring in the decay of the daughter isotopes. These activities at all positions were compared to the activities at 0 cm to give the attenuations. The weighted average of the attenuations of all foils at each position were calculated, where the weighting was determined by the uncertainties.

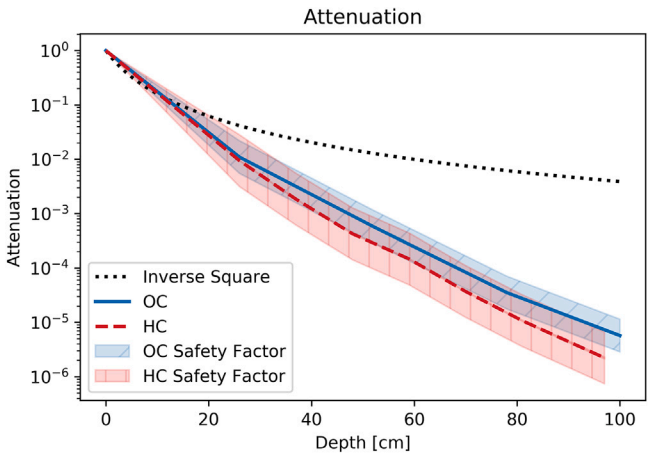

Fig. 12. The attenuations for both concretes including the uncertainties and safety ranges. The inverse square relation is also plotted for reference.

The uncertainties were propagated through and the resulting attenuations are shown in Fig. 12. Safety factors were calculated from the C/E results (Section 3.3) to be 2 for OC and 3 for HC, these are also shown in the plot. The safety factors were calculated by averaging the upper and lower limits of the C/E results for all of the reactions including the uncertainties and using the largest values to be conservative.

For both concretes, the activities of the foils show general exponential decreases with attenuations of ~ 5–6 magnitudes over 100 cm, with slightly more attenuation provided by HC. These attenuations include all of the experimental results, including the unusually high activity for ^{48}Sc in HC. The calculation of the attenuations did not account for the different foils' responses to the neutron spectrum, therefore, the averaged attenuations are simplifications. The inverse square relation is also plotted to show the attenuation caused purely by the concretes, which was approximately 3–4 orders of magnitude over 100 cm.

3.2. Sensitivity and uncertainty results

It was found that the results were sensitive to all of the sources of uncertainty listed in Section 2.8 and so each had a significant contribution to the overall uncertainty. The individual uncertainties were added in quadrature to give the overall uncertainties. These are shown with the error bars in Section 3.3. The error bars also include contributions from the known uncertainties from the experiment and calculations such as 5% uncertainty on the experimental proton beam current and the statistical uncertainty from the Monte-Carlo simulations.

The independent, nuclear data sensitivity and uncertainty analysis performed in [27] found that the results were most sensitive to the cross-sections of iron, oxygen, hydrogen and calcium. The sensitivity results for HC for all foils in position 3 and the In foil additionally at positions 6 and 7 are shown in Table 7.

Among the neutron nuclear data libraries only the FENDL-3.2 library [21], extending up to 55 MeV, covered the required neutron energy range. JEFF-4.0 [31] and in particular ENDF/B-VIII.1 [32] libraries were found not to be suitable for these applications since the cross-section evaluations for several important isotopes (including e.g. ^{1}H, ^{23}Na, $^{24-26}$Mg, $^{39-41}$K) were only available up to 20 MeV. To determine the nuclear data implied uncertainty in the calculated saturated reaction rates, the information on the covariance matrices is needed in addition to the sensitivity profiles. However, the availability and quality of covariances in the FENDL-3.2 library is rather poor. Furthermore, the covariance data are limited to up to 20 MeV. The uncertainties, to be considered as only informative due to the above reasons, are listed in Table 8.

Table 7
Energy integrated sensitivities of the reaction rates measured at the positions P3, P6 and P7 in the HC experimental mock-up to the total cross-sections of the most sensitive isotopes present (^{16}O,^{1}H,^{56}Fe and^{40}Ca). The sensitivities were calculated using the SUSD3D/DORT sequence and 211-group FENDL-3.2 cross sections.

Isotope	Sensitivity [%/%]						
	In P3	In P6	In P7	Al P3	^{48}Ti (n, p) P3	Fe P3	Au P3
^{56}Fe	−1.19	−2.58	−3.05	−1.22	−1.20	−1.24	−0.51
^{16}O	−0.81	−1.76	−2.08	−1.13	−1.13	−1.07	−0.27
^{1}H	−0.50	−0.82	−0.91	−0.17	−0.17	−0.19	−0.68
^{40}Ca	−0.11	−0.25	−0.29	−0.13	−0.12	−0.13	+0.06

Table 8
Comparison of uncertainties in the calculated reaction rates at the detector positions P3 (and P6/P7 for In), estimated using DORT/SUSD3D sequence of codes, the FENDL-3.2 211-group transport cross sections and covariance matrices, and IRDFF-II dosimetry cross sections. The values correspond to the uncertainty calculated from partial reaction covariances. σ_D is uncertainty in detector response function taken from IRDFF-II.

Isotope	Uncertainty [%] (DORT/SUSD3D/FENDL-3.2)						
	In P3	In P6	In P7	Al P3	^{48}Ti (n, p) P3	Fe P3	Au P3
Total	2.2	5.3	6.5	10.6	12.1	10.1	2.2
^{56}Fe	1.7	4.2	5.1	1.6	1.5	4.2	2.2
^{16}O	1.2	3.0	3.7	10.5	11.1	9.1	0.2
^{1}H	0.9	1.5	1.7	0.4	0.4	0.4	0.2
σ_D	1.6	1.6	1.6	0.5	3.6	1.9	1.1

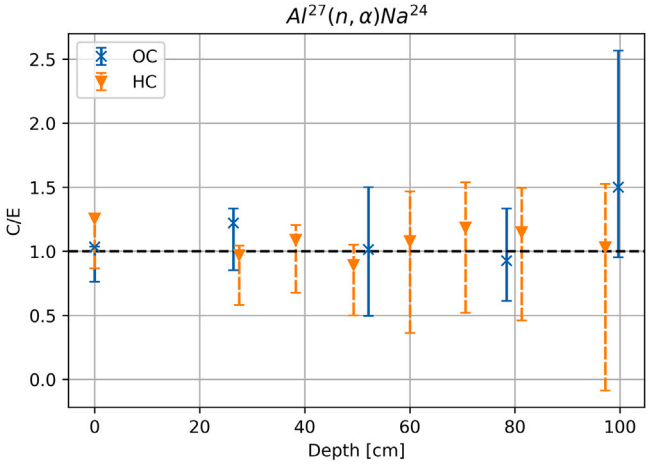

Fig. 13. The C/E results and the associated uncertainties for the ^{27}Al (n, α) ^{24}Na reaction for both concretes.

The sensitivity profiles for the reaction rates of the foils were calculated for the sensitivities to the detector response functions and the total, elastic and inelastic transport cross-sections of ^{56}Fe, ^{16}O and ^{1}H. The sensitivity profiles for the aluminium, iron and titanium foil reaction rates all had similar energy ranges and shapes. This suggests that they were essentially measuring the same neutron energies despite the slightly different threshold energies. Therefore, any differences observed in the C/Es between these foils generally would not be attributed to the transport cross-section data.

3.3. C/E results

The C/E results for the reactions listed in Table 2 for both concretes with the uncertainties as quantified above are shown in Figs. 13–18.

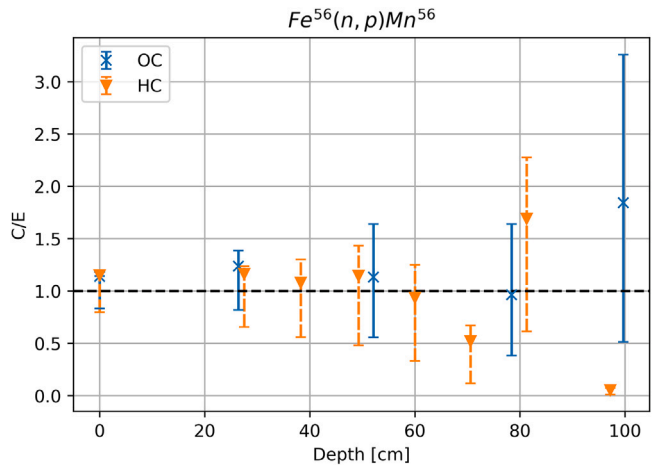

Fig. 14. The C/E results and the associated uncertainties for the ^{56}Fe (n, p) ^{56}Mn reaction for both concretes.

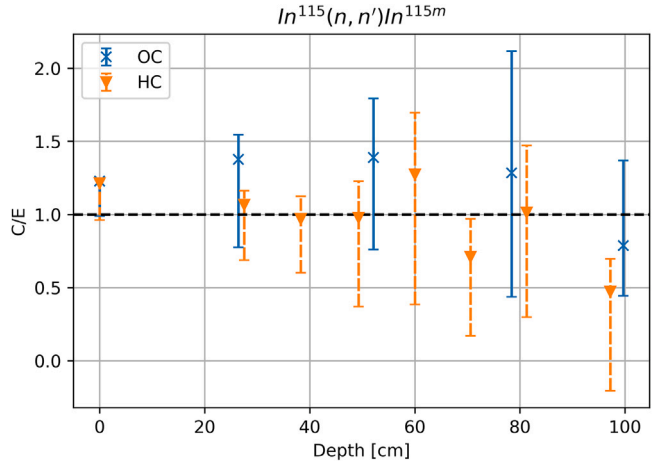

Fig. 15. The C/E results and the associated uncertainties for the ^{115}In (n, n') ^{115m}In reaction for both concretes.

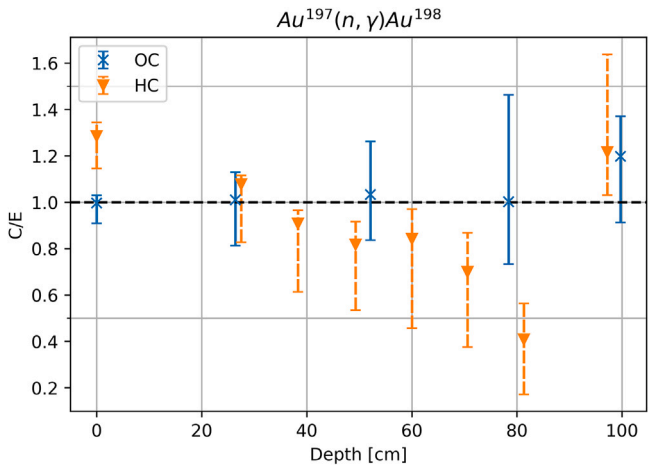

Fig. 16. The C/E results and the associated uncertainties for the ^{197}Au (n, γ) ^{198}Au reaction for both concretes.

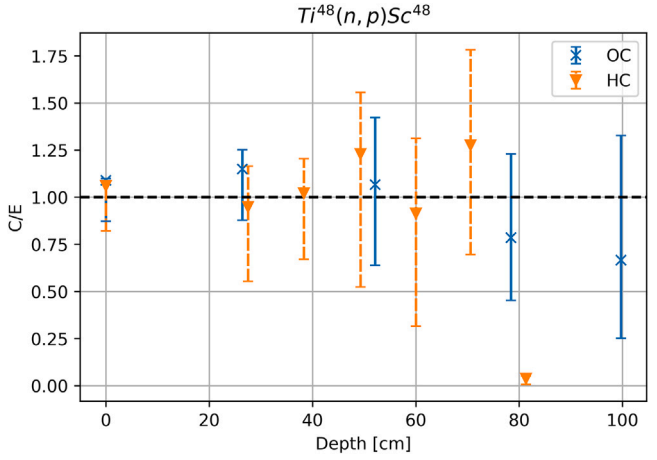

Fig. 17. The C/E results and the associated uncertainties for the ^{48}Ti (n, p) ^{48}Sc reaction for both concretes.

As shown in Fig. 13, the aluminium foils reaction showed C/E agreement for both concretes throughout the depths. The uncertainties at the back of the mock-ups were large. All of the investigated sources of uncertainty listed in Section 2.8 contributed significantly to these rear uncertainties but the statistical uncertainties from the Monte Carlo simulations dominated.

As shown in Fig. 14, the iron foils reaction showed C/E agreement for OC throughout the mock-up and for most of the HC results. For HC, there are a couple of underpredictions towards the back of the mock-up. The HC was prepared with a magnetite aggregate unlike the OC and so the presence of iron was much higher in HC than in OC, as shown in Table 1. The cause of the C/E discrepancies in HC could be because of neutron removal due to iron. The simulations may have overpredicted the amount of iron present in HC or overpredicted the cross-sections of these neutron removal reactions. Which would be why the discrepancy was only observed for HC. The C/E agreement for OC implies that the cross-sections for specifically the ^{56}Fe (n, p) ^{56}Mn reaction used in the modelling were correct within the uncertainties. The uncertainties on the low C/E HC values were much smaller than the respective OC uncertainties. However, the relative uncertainties were broadly similar for both OC and HC. That the HC values were low therefore also gave low uncertainties.

As shown in Fig. 15, the indium foils reaction showed general C/E agreement for both concretes albeit with large uncertainties. There are a couple of underpredictions in the second half of the HC mock-up. This reaction has a low energy threshold and so there is slightly poor understanding of the low-energy region in the modelling for HC, similar to what is observed with the gold reaction but to a lesser extent. The low-energy region being difficult to accurately model is also the cause of the large uncertainties for both concretes.

As shown in Fig. 16, the gold foils reaction showed C/E agreement for OC but for HC the calculations overpredict the activity at the front of the mock-up and then the C/E decreases consistently such that the calculations underpredict the activity at most depths until the back of the mock-up where an overprediction is again observed. This is the only non-threshold reaction investigated, and the neutron thermal region is most susceptible to scattering in the experiment. The thermal region appears to be poorly modelled for HC but there are many possibilities for the cause, including neutron scattering phenomena. Neutron scattering particularly effects the thermal region because when high energy neutrons undergo inelastic scattering, their energies trend towards thermal energies. Since this scattering can occur anywhere in the geometry and neutrons will undergo numerous scatters, it is difficult to accurately model in Monte-Carlo simulations as any inaccuracies in the geometry and material modelling will have an effect. Therefore, some inaccuracy in the HC modelling is inferred.

As shown in Fig. 17, the (n,p) reaction in the titanium foils showed C/E agreement for both concretes albeit with large uncertainties. The

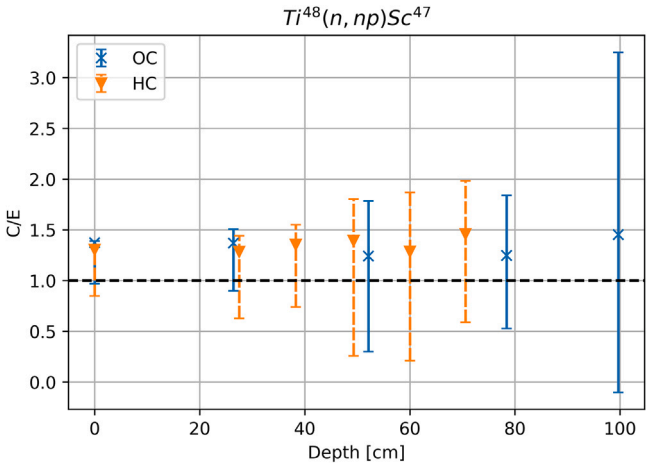

Fig. 18. The C/E results and the associated uncertainties for the ^{48}Ti (n, np) ^{47}Sc reaction for both concretes.

result at ~ 80 cm for HC is due to the relatively large activity measured in the experiment at this position. The most likely cause of this is some fault in the spectrometry since the other experimental results and the simulations do not predict this. The activities towards the back of the HC mock-up were too low to be measured.

As shown in Fig. 18, the (n,np) reaction in the titanium foils showed C/E agreement for both concretes.

4. Discussion

The OC C/E results show good agreement overall, with all datapoints exhibiting agreement within the uncertainties. The HC C/E results, on the other hand, exhibit disagreements for low and thermal neutron energy regions throughout the mock-up and also mid-range neutron energies in the rear half of the mock-up.

The ^{56}Fe (n, p) ^{56}Mn, ^{48}Ti (n, p) ^{48}Sc and ^{27}Al (n, α) ^{24}Na reactions have similar threshold energies, 3.0, 3.3 and 3.2 MeV respectively, see Table 2. The nuclear data sensitivity analysis showed that these three reactions were essentially measuring the same neutron energies. The OC C/E results for these three reactions were good. For HC, however, while the ^{24}Na C/E results were also good, there were some disagreements in the C/E results for the other two reactions. The ^{48}Sc experimental activity was relatively very high at 81 cm. This was not observed for ^{56}Mn nor ^{24}Na, and there was no trend in the ^{48}Sc activities to predict this. The threshold energies of the ^{48}Sc reactions is too high for room-scattered neutrons to be the main factor in the large activity observed, furthermore, if room-scatter was dominant then the activity at 100 cm would be detectable. It is concluded that this high activity was not an effect of the neutron transport but rather an anomalous result due to the spectrometry. Further investigation is needed to verify this. Also for HC, the ^{56}Mn C/E results had a couple of underpredictions towards the rear of the mock-up. These were not due to relatively large activities like for ^{48}Sc. Disregarding the ^{48}Sc result at 81 cm, the C/E underpredictions were not observed for ^{24}Na nor ^{48}Sc. This would generally imply that the ^{56}Mn C/E underpredictions cannot be attributed to the neutron spectrum. However, a significant difference between the OC and HC mock-ups was the greatly increased content of Fe in HC. It is possible that Fe content in the HC simulations was not accurately modelled. This would have had a greater effect on the Fe foil results than the Ti and Al foils because even though the threshold energies are similar, it is the same element and therefore has the exact same neutron interaction cross-section. The nuclear data sensitivity analysis also showed that the results were most sensitive to the cross-sections of iron, oxygen, hydrogen and calcium. The greatly increased iron composition in HC compared to OC suggests that the iron cross-section could be source of the disagreement observed in the ^{56}Mn results for HC.

The low and thermal neutron energy regions disagreements for HC have a number of possible contributing factors due to the increased sensitivity of these regions to neutron scattering. However, the good agreement observed for these regions for OC implies that the source of the discrepancies arises from the HC modelling. Again, the major composition increase from OC to HC is the presence of iron. This suggests that there are neutron–iron interactions which were not accurately represented in the simulations. Even though the pre-analysis determined not to use extrinsic shielding for the mock-ups, from the experiments it was clear that accurate modelling of the complete experimental hall and thus the neutron scattering and thus the low and thermal neutron energy regions was very difficult. Therefore, shielding against room-scatter neutrons would have benefitted the experiment and reduced uncertainties. This is particularly important for the low and thermal neutron energy regions but also the entire neutron spectrum at the back of the mock-ups, where the effect of scattered neutrons on the experimental activities was observed.

To completely understand the changes in the neutron spectrum throughout the mock-ups, spectrum unfolding would need to be conducted. The secondary reactions of the foils would need to be investigated to see if there are sufficient pathways for reliable unfolding.

Overall, the C/E disagreements for the HC results suggest disparities between the experiment and the computational representation. Although efforts were made to quantify the uncertainties, possible causes are inaccurate composition of the concrete, inaccurate geometrical modelling and inaccurate nuclear data. It is likely that it is some combination of all of these factors. The large increase of iron in HC compared to OC, coupled with the sensitivity of the results to the cross-section of iron, suggest that this may be a large contributor to the disagreements.

The radiation transport statistical uncertainties were large for all of the reactions at the back of the mock-ups, contributing to the large uncertainties observed in the C/E results. In order to account for the scattered neutrons from all of the experiment hall, a targeted mesh global WW was used for variance reduction but the large statistical uncertainties at the back of the mock-ups were not completely mitigated. Due to the SSR/W source method, the number of neutron histories that could be simulated was limited and could not be increased to improve the statistics. To improve this, the SSR/W source should be replicated in the MCNP SDEF format. Initial efforts to do so were made but the results were not accurate enough for these analyses and so it was abandoned in the interest of time. Having the source in SDEF format would also increase the repeatability of the analysis and would be necessary for inclusion in the SINBAD database.

The quantified uncertainties in the C/E results were often asymmetric with the lower error value being larger than the upper value. The main contributor to this was the uncertainty due to the proton transport library. The flux simulated with JENDL-4.0/HE was lower than with ENDF7PROT [4] and the datapoints were calculated with ENDF7PROT, therefore the lower error bound accounts for the JENDL-4.0/HE library.

A number of factors contributed to the quantified uncertainties which were large and impose conservative safety factors for subsequent simulations regarding these concretes. In particular, the difficulty in minimising the uncertainties due to the source characterisation is highlighted. Furthermore, the sensitivity analysis concluded that the results were very sensitive to the geometrical modelling of the experiment and, therefore, the difficulty in accurately modelling the geometry of the experiment introduced significant uncertainties.

The absolute neutron attenuation observed was similar for both concretes, demonstrating minimal improvement from using HC. This is a slightly surprising result, even just considering the marked increased density of HC compared to OC. The economic cost of producing the HC samples for this experiment was far greater than for OC. This increased cost, therefore, is not justified from a neutron shielding perspective. This work did not investigate gamma shielding.

5. Conclusion

Neutron shielding experiments were performed for OC and HC using activation foil diagnostics. The neutron attenuations provided by the concretes were similar across the range of the neutron spectrum. Simulations were performed to replicate the experiments and provide C/E results. Sensitivities and uncertainties on the experimental and calculated results were quantified. 100% of the OC C/E results and 73% of the HC results showed agreement within the uncertainties. The HC disagreements were particularly for the thermal and mid-range neutron energy regions, suggesting inaccuracies in the modelling of that concrete. Although the C/E results for OC were good, this analysis recommends a safety factor of 2 for future analysis regarding OC, mainly due to the uncertainties. Due to the uncertainties and disagreements in the HC results, a safety factor of 3 is recommended for future analysis regarding HC.

CRediT authorship contribution statement

Haridev Chohan: Writing – review & editing, Writing – original draft, Visualization, Validation, Supervision, Software, Resources, Project administration, Methodology, Investigation, Formal analysis, Data curation, Conceptualization. **Martin Ansorge:** Writing – review & editing, Validation, Supervision, Resources, Project administration, Methodology, Investigation, Formal analysis, Data curation, Conceptualization. **Yuefeng Qiu:** Writing – review & editing, Validation, Supervision, Resources, Project administration, Methodology, Investigation, Funding acquisition, Conceptualization. **Tomasz Piotrowski:** Writing – review & editing, Resources, Methodology, Investigation, Formal analysis, Data curation, Conceptualization. **María José Martínez-Echevarría Romero:** Writing – review & editing, Resources, Methodology, Investigation, Formal analysis, Data curation. **Ocean Wong:** Writing – review & editing, Validation, Software, Methodology, Investigation, Formal analysis, Data curation, Conceptualization. **Ivan Kodeli:** Writing – review & editing, Methodology, Investigation, Formal analysis, Conceptualization. **Joseph Neilson:** Writing – review & editing, Validation, Methodology, Formal analysis, Data curation. **Kimberley Lennon:** Writing – review & editing, Validation, Project administration, Methodology, Formal analysis, Data curation. **Robin Smith:** Writing – review & editing, Validation, Resources, Project administration, Methodology, Funding acquisition, Formal analysis, Data curation. **Radomír Běhal:** Writing – review & editing, Methodology, Data curation. **Anastasia Cassisa:** Methodology, Data curation. **Vadim Glagolev:** Writing – review & editing, Methodology, Data curation. **Daniil Koliadko:** Methodology, Data curation. **Ján Kozic:** Writing – review & editing, Methodology, Data curation. **Jaromír Mrázek:** Writing – review & editing, Methodology, Data curation. **Jan Novák:** Writing – review & editing, Methodology, Data curation. **Eva Šimečková:** Writing – review & editing, Methodology, Data curation. **Milan Štefánik:** Writing – review & editing, Methodology, Data curation. **Callum Grove:** Writing – review & editing, Validation, Methodology, Formal analysis. **Timothy Germany:** Validation, Formal analysis. **Tim Eade:** Supervision, Project administration, Investigation, Conceptualization. **Mark Gilbert:** Writing – review & editing, Supervision, Project administration, Investigation, Conceptualization. **Chantal Shand:** Supervision. **Allan Harte:** Supervision, Funding acquisition.

Declaration of competing interest

The authors declare that they have no known competing financial interests or personal relationships that could have appeared to influence the work reported in this paper.

Acknowledgements

This work has been carried out within the framework of the EUROfusion Consortium, funded by the European Union via the Euratom Research and Training Programme (Grant Agreement No 101052200 — EUROfusion) and from the EPSRC [grant number EP/W006839/1]. To obtain further information on the data and models underlying this paper please contact PublicationsManager@ukaea.uk*. Views and opinions expressed are however those of the author(s) only and do not necessarily reflect those of the European Union or the European Commission. Neither the European Union nor the European Commission can be held responsible for them.

The measurements were carried out at the infrastructure CANAM of the NPI CAS Řež, supported by the Ministry of Education, Youth and Sports of the Czech Republic under the project LM2015056.

This work was supported by the UK Science and Technology Facilities Council (STFC) [grant numbers ST/V001086/1 and ST/Y000331/1].

Data availability

Data will be made available on request.

References

[1] W. Królas, A. Ibarra, F. Arbeiter, F. Arranz, D. Bernardi, M. Cappelli, J. Castellanos, T. Dézsi, H. Dzitko, P. Favuzza, A. García, J. Gutiérrez, M. Lewitowicz, A. Maj, F. Martin-Fuertes, G. Micciché, A. Muñoz, F. Nitti, T. Pinna, I. Podadera, J. Pons, Y. Qiu, R. Román, M. Toth, A. Zsakai, The IFMIF-DONES fusion oriented neutron source: evolution of the design, Nucl. Fusion 61 (12) (2021) 125002, http://dx.doi.org/10.1088/1741-4326/ac318f.

[2] Y. Qiu, T. Berry, K. Ambrožic, B. Bieńkowska, H. Chohan, A. Cufar, D. Dworak, B. Kos, V. Lopez Ochoa, F. Mota, M.J. Martinez-Echevarria, I. Álvarez Castro, T. Piotrowski, A.J. López Revelles, A. Serikov, G. Stankunas, A. Tidikas, L. Taling, G. Tracz, U. Wiącek, G. Žerovnik, M. Ansorge, M. Anguiano, T. Dezsi, J. García, D. Jiménez-Rey, M. Kepniak, E. Mendoza Cembranos, J. Malec, J.H. Park, F. Ogando, J. Martínez-Serrano, Status of DONES neutronics, source terms analyses and radiation protections, Nucl. Fusion (2025) URL http://iopscience.iop.org/article/10.1088/1741-4326/addeda.

[3] Y. Qiu, M. Ansorge, I. Álvarez, K. Ambrožič, T. Berry, B. Bieńkowska, H. Chohan, A. Čufar, D. Dworak, T. Dezsi, T. Eade, J. García, D. Jimenez-Rey, I. Lengar, A. Lopez-Revelles, V. Lopez, E. Mendoza, F. Mota, M. Martinez-Echevarria, F. Ogando, J. Park, T. Piotrowski, A. Serikov, G. Stankunas, A. Tidikas, G. Tracz, G. Žerovnik, F. Arbeiter, F. Arranz, S. Becerril, P. Cara, D. Bernardi, J. Castellanos, J. Gutiérrez, A. Ibarra, W. Królas, J. Maestre, F. Martín-Fuertes, J. Marugán, G. Micciché, J. Martínez-Serrano, F. Nitti, I. Podadera, U. Wiącek, U. Fischer, Overview of recent advancements in IFMIF-dones neutronics activities, Fusion Eng. Des. 201 (2024) 114242, http://dx.doi.org/10.1016/j.fusengdes.2024.114242.

[4] M. Majerle, M. Ansorge, P. Bém, D. Koliadko, J. Mrázek, J. Novák, E. Šimečková, M. Štefánik, M. Košťál, Z. Matěj, H. Chohan, O. Wong, Measurements of the neutron spectra from the p+be neutron generator of the NPI CAS, Nucl. Instrum. Methods Phys. Res. Sect. A: Accel. Spectrometers, Detect. Assoc. Equip. 1053 (2023) 168314, http://dx.doi.org/10.1016/j.nima.2023.168314, URL https://www.sciencedirect.com/science/article/pii/S0168900223003042.

[5] T. Piotrowski, M.J.M.-E. Romero, P. Prochoń, M.L. Alonso, R. Michalczyk, A. Arvizu-Montes, Ł. Ciupiński, S.B. Jarque, K. Józefiak, Y. Qiu, M. Ansorge, H. Chohan, M. Wojtkowska, Optimization and evaluation of structural and shielding concrete for IFMIF-DONES, Nucl. Mater. Energy 38 (2024) 101597, http://dx.doi.org/10.1016/j.nme.2024.101597, URL https://www.sciencedirect.com/science/article/pii/S235217912400019X.

[6] M. Angelone, D. Flammini, S. Loreti, F. Moro, M. Pillon, R. Villari, Copper benchmark experiment at the frascati neutron generator for nuclear data validation, Fusion Eng. Des. 109–111 (2016) 843–847, http://dx.doi.org/10.1016/j.fusengdes.2016.01.065, Proceedings of the 12th International Symposium on Fusion Nuclear Technology-12 (ISFNT-12), URL https://www.sciencedirect.com/science/article/pii/S0920379616300655.

[7] P. Batistoni, M. Angelone, M. Martone, M. Pillon, V. Rado, A. Santamarina, I. Abidi, B. Gastaldi, M. Martini, J. Marquette, The bulk shielding benchmark experiment at the frascati neutron generator (FNG), Fusion Eng. Des. 28 (1995) 504–514, http://dx.doi.org/10.1016/0920-3796(95)90077-2, Proceedings of the Third International Symposium on Fusion Nuclear Technology, URL https://www.sciencedirect.com/science/article/pii/0920379695900772.

[8] I.A. Kodeli, E. Sartori, SINBAD – radiation shielding benchmark experiments, Ann. Nucl. Energy 159 (2021) 108254, http://dx.doi.org/10.1016/j.anucene.2021.108254.

[9] C. Werner, et al., MCNP users manual - code version 6.2, 2017, LA-UR-17-29981.
[10] M. Angelone, P. Batistoni, F. Moro, M. Pillon, R. Villari, M. Laubenstein, M. Loughlin, Neutronics analysis and nuclear heating measurement up to the TFC in a mock-up of the ITER inboard shield, Fusion Eng. Des. 87 (5) (2012) 910–915, http://dx.doi.org/10.1016/j.fusengdes.2012.02.045, Tenth International Symposium on Fusion Nuclear Technology (ISFNT-10), URL https://www.sciencedirect.com/science/article/pii/S0920379612001056.
[11] I.J. Curl, A.K. McCracken, P.C. Miller, JANUS Phase I (Neutron Transport Through Mild and Stainless Steel), Tech. Rep., AEA Technology, 1986.
[12] L.A. Currie, Limits for qualitative detection and quantitative determination. application to radiochemistry, Anal. Chem. 40 (3) (1968) 586–593, http://dx.doi.org/10.1021/ac60259a007.
[13] J.-C. Sublet, J. Eastwood, J. Morgan, M. Gilbert, M. Fleming, W. Arter, FISPACT-II: An advanced simulation system for activation, transmutation and material modelling, Nucl. Data Sheets 139 (2017) 77–137, http://dx.doi.org/10.1016/j.nds.2017.01.002, Special Issue on Nuclear Reaction Data.
[14] O. Wong, R. Smith, C.R. Nobs, A.M. Bruce, Optimising foil selection for neutron activation systems, J. Fusion Energy 41 (2022) http://dx.doi.org/10.1007/s10894-022-00324-w.
[15] A. Davis, R. Pampin, Benchmarking the MCR2S system for high-resolution activation dose analysis in ITER, Fusion Eng. Des. 85 (1) (2010) 87–92, http://dx.doi.org/10.1016/j.fusengdes.2009.07.002, URL https://www.sciencedirect.com/science/article/pii/S0920379609002518.
[16] Genie 2000 spectroscopy software: Customization tools V3.0, 2004.
[17] jaromrax, Gregory-online, 2023, URL https://pypi.org/project/gregory-online/0.3.7/.
[18] S. Chen, B. Wu, Z. Dong, S. Zhou, G. Sun, L. He, D. Yao, S. Yu, Q. Gan, L. Hao, J. Song, P. Long, Y. Li, J. Jiang, F. Wang, L. Hu, Y. Wu, FDS Consortium, Development of TopMC 1.0 for nuclear technology applications, EPJ Nucl. Sci. Technol. 11 (2025) 6, http://dx.doi.org/10.1051/epjn/2024033.
[19] S.W. Mosher, S.R. Johnson, A.M. Bevill, A.M. Ibrahim, C.R. Daily, T.M. Evans, J.C. Wagner, J.O. Johnson, R.E. Grove, ADVANTG - An Automated Variance Reduction Parameter Generator, Tech. Rep., Oak Ridge National Laboratory (ORNL), Oak Ridge, TN (United States), 2015.
[20] M. Chadwick, P. Obložinský, M. Herman, N. Greene, R. McKnight, D. Smith, P. Young, R. MacFarlane, G. Hale, S. Frankle, A. Kahler, T. Kawano, R. Little, D. Madland, P. Moller, R. Mosteller, P. Page, P. Talou, H. Trellue, S. van der Marck, ENDF/B-VII.0: Next Generation Evaluated Nuclear Data Library for Nuclear Science and Technology, Nucl. Data Sheets 107 (2006) 2931–3060, http://dx.doi.org/10.1016/j.nds.2006.11.001.
[21] G. Schnabel, D. Aldama, T. Bohm, U. Fischer, S. Kunieda, A. Trkov, C. Konno, R. Capote, A. Koning, S. Breidokaite, T. Eade, M. Fabbri, D. Flammini, L. Isolan, I. Kodeli, M. Košťál, S. Kwon, D. Laghi, D. Leichtle, S. Nakayama, M. Ohta, L. Packer, Y. Qiu, S. Sato, M. Sawan, M. Schulc, G. Stankunas, M. Sumini, A. Valentine, R. Villari, A. Žohar, FENDL: A library for fusion research and applications, Nucl. Data Sheets 193 (2024) 1–78, http://dx.doi.org/10.1016/j.nds.2024.01.001, Special Issue on Nuclear Reaction Data, URL https://www.sciencedirect.com/science/article/pii/S0090375224000012.
[22] G. Bailey, D. Foster, P. Kanth, M. Gilbert, The FISPACT-II User Manual, Tech. Rep., United Kingdom Atomic Energy Authority (UKAEA), Oxon, (United Kingdom), 2023.
[23] A. Trkov, P. Griffin, S. Simakov, L. Greenwood, K. Zolotarev, R. Capote, D. Aldama, V. Chechev, C. Destouches, A. Kahler, C. Konno, M. Koštál, M. Majerle, E. Malambu, M. Ohta, V. Pronyaev, V. Radulović, S. Sato, M. Schulc, E. Šimečková, I. Vavtar, J. Wagemans, M. White, H. Yashima, IRDFF-II: A new neutron metrology library, Nucl. Data Sheets 163 (2020) 1–108, http://dx.doi.org/10.1016/j.nds.2019.12.001, URL https://www.sciencedirect.com/science/article/pii/S0090375219300687.
[24] J.C. Sublet, A. Koning, D. Rochman, TENDL-2017: The Making of Multi-Faceted Technological Nuclear Data Library - 25340, American Nuclear Society - ANS, 555 North Kensington Avenue, La Grange Park, IL 60526 (United States), 2018, URL https://www.osti.gov/biblio/23055070.
[25] S. Kunieda, O. Iwamoto, N. Iwamoto, F. Minato, T. Okamoto, T. Sato, H. Nakashima, Y. Iwamoto, H. Iwamoto, F. Kitatani, et al., Overview of JENDL-4.0/HE and benchmark calculations, 2016, pp. 41–46, http://dx.doi.org/10.11484/jaea-conf-2016-004.
[26] A. Plompen, O. Cabellos, C. De Saint Jean, M. Fleming, A. Algora, M. Angelone, P. Archier, E. Bauge, O. Bersillon, A. Blokhin, F. Cantargi, A. Chebboubi, C. Diez, H. Duarte, E. Dupont, J. Dyrda, B. Erasmus, L. Fiorito, U. Fischer, D. Flammini, D. Foligno, M. Gilbert, J. Granada, W. Haeck, F. Hambsch, P. Helgesson, S. Hilaire, I. Hill, M. Hursin, R. Ichou, R. Jacqmin, B. Jansky, C. Jouanne, M. Kellett, D. Kim, H. Kim, I. Kodeli, A. Koning, A. Konobeyev, S. Kopecky, B. Kos, A. Krasa, L. Leal, N. Leclaire, P. Leconte, Y. Lee, H. Leeb, O. Litaize, M. Majerle, J. Marquez Damian, F. Michel-Sendis, R. Mills, B. Morillon, G. Noguere, M. Pecchia, S. Pelloni, P. Pereslavtsev, R. Perry, D. Rochman, R. Roehrmoser, P. Romain, P. Romojaro, D. Roubtsov, P. Sauvan, P. Schillebeeckx, K. Schmidt, O. Serot, S. Simakov, I. Sirakov, H. Sjöstrand, A. Stankovskiy, J. Sublet, P. Tamagno, A. Trkov, S. Van Den Marck, F. Velarde, R. Villari, K. Yokoyama, G. Zerovnik, The joint evaluated fission and fusion nuclear data library, JEFF-3.3, Eur. Phys. J. A 56 (2020) 181, http://dx.doi.org/10.1140/epja/s10050-020-00141-9(online), URL https://rdcu.be/b5CJV.
[27] I. Kodeli, A. Čufar, Sensitivity and Uncertainty Study of the IFMIF-DONES Shielding Mock-Up Experiment, Tech. rep., Jožef Stefan Institute - EUROfusion, 2025.
[28] I.A. Kodeli, S. Slavič, SUSD3D computer code as part of the XSUN-2017 windows interface environment for deterministic radiation transport and cross-section sensitivity-uncertainty analysis, Sci. Technol. Nucl. Install. 2017 (1) (2017) 1264736, http://dx.doi.org/10.1155/2017/1264736, arXiv:https://onlinelibrary.wiley.com/doi/pdf/10.1155/2017/1264736, URL https://onlinelibrary.wiley.com/doi/abs/10.1155/2017/1264736.
[29] I.A. Kodeli, XSUN-2022/SUSD3D n/sitivity-uncertainty code package with recent JEFF-3.3 and ENDF/B-VIII.0 covariance data, EPJ Web Conf. 281 (2023) 00013, http://dx.doi.org/10.1051/epjconf/202328100013.
[30] I. Kodeli, Multidimensional deterministic nuclear data sensitivity and uncertainty code system: Method and application, Nucl. Sci. Eng. 138 (1) (2001) 45–66, http://dx.doi.org/10.13182/NSE00-43, arXiv:10.13182/NSE00-43.
[31] Joint Evaluated Fission and Fusion Project, JEFF-4.0 evaluated data: neutron data, 2025, http://dx.doi.org/10.82555/e9ajn-a3p20.
[32] G.P.A. Nobre, R. Capote, M.T. Pigni, A. Trkov, C.M. Mattoon, D. Neudecker, D.A. Brown, M.B. Chadwick, A.C. Kahler, N.A. Kleedtke, M. Zerkle, A.I. Hawari, C.W. Chapman, N.C. Fleming, J.L. Wormald, K. Ramić, Y. Danon, N.A. Gibson, P. Brain, M.W. Paris, G.M. Hale, I.J. Thompson, D.P. Barry, I. Stetcu, W. Haeck, A.E. Lovell, M.R. Mumpower, G. Potel, K. Kravvaris, G. Noguere, J.D. McDonnell, A.D. Carlson, M. Dunn, T. Kawano, D. Wiarda, I. Al-Qasir, G. Arbanas, R. Arcilla, B. Beck, D. Bernard, R. Beyer, J.M. Brown, O. Cabellos, R.J. Casperson, Y. Cheng, E.V. Chimanski, R. Coles, M. Cornock, J. Cotchen, J.P.W. Crozier, D.E. Cullen, A. Daskalakis, M.A. Descalle, D.D. DiJulio, P. Dimitriou, A.C. Dreyfuss, I. Durán, R. Ferrer, T. Gaines, V. Gillette, G. Gert, K.H. Guber, J.D. Haverkamp, M.W. Herman, J. Holmes, M. Hursin, N. Jisrawi, A.R. Junghans, K.J. Kelly, H.I. Kim, K.S. Kim, A.J. Koning, M. Koštál, B.K. Laramee, A. Lauer-Coles, L. Leal, H.Y. Lee, A.M. Lewis, J. Malec, J.I.M. Damián, W.J. Marshall, A. Mattera, G. Muhrer, A. Ney, W.E. Ormand, D.K. Parsons, C.M. Percher, V.G. Pronyaev, A. Qteish, S. Quaglioni, M. Rapp, J.J. Ressler, M. Rising, D. Rochman, P.K. Romano, D. Roubtsov, G. Schnabel, M. Schulc, G.J. Siemers, A.A. Sonzogni, P. Talou, J. Thompson, T.H. Trumbull, S.C. van der Marck, M. Vorabbi, C. Wemple, K.A. Wendt, M. White, R.Q. Wright, ENDF/B-VIII.1: updated nuclear reaction data library for science and applications, 2025, arXiv:2511.03564, URL https://arxiv.org/abs/2511.03564.